

Rethinking the Mean Teacher Strategy from the Perspective of Self-paced Learning

Pengchen Zhang^{*1}, Alan J.X. Guo^{*†1}, Sipin Luo², Zhe Han³, and Lin Guo²

¹Center for Applied Mathematics, Tianjin University

²Department of Radiology, Tianjin Hospital of Tianjin University

³Department of Hip Trauma, Tianjin Hospital of Tianjin University

Abstract

Semi-supervised medical image segmentation has attracted significant attention due to its potential to reduce manual annotation costs. The mean teacher (MT) strategy, commonly understood as introducing smoothed, temporally lagged consistency regularization, has demonstrated strong performance across various tasks in this field. In this work, we reinterpret the MT strategy on supervised data as a form of self-paced learning, regulated by the output agreement between the temporally lagged teacher model and the ground truth labels. This idea is further extended to incorporate agreement between a temporally lagged model and a cross-architectural model, which offers greater flexibility in regulating the learning pace and enables application to unlabeled data. Specifically, we propose dual teacher-student learning (DTSL), a framework that introduces two groups of teacher-student models with different architectures. The output agreement between the cross-group teacher and student models is used as pseudo-labels, generated via a Jensen-Shannon divergence-based consensus label generator (CLG). Extensive experiments on popular datasets demonstrate that the proposed method consistently outperforms existing state-of-the-art approaches. Ablation studies further validate the effectiveness of the proposed modules.

1 Introduction

Medical image segmentation plays a vital role in computer-aided diagnosis [1; 2; 3]. Compared to natural images, medical images typically require more precise annotations, which must be performed by experienced experts. This is an effort-intensive and time-consuming process and hinders the progress of medical image segmentation [4]. To address this, semi-supervised medical image segmentation (SSMIS) has emerged as a promising and efficient approach. It leverages unlabeled samples to supplement supervised learning on a limited set of labeled data [5; 6; 7; 8; 9].

In SSMIS, the mean teacher (MT) strategy and its variants are widely adopted. Two models with identical architecture are instantiated as the teacher and student. The student is trained using both human-annotated labels and pseudo-labels generated by the teacher. The teacher model is updated via an exponential moving average (EMA) of the student’s weights,

$$\Theta_t^T = \omega \Theta_{t-1}^T + (1 - \omega) \Theta_t^S, \quad (1)$$

where Θ_t^S is the weight of the student model at step t , and Θ_{t-1}^T is the weight of the teacher model at step $t - 1$. This strategy has demonstrated strong performance in SSMIS and has inspired numerous successful extensions [10; 7; 11].

^{*} Equal contribution. [†] Corresponding author: jiaxiang.guo@tju.edu.cn

Consistency regularization has been regarded as the primary factor behind the effectiveness of the MT strategy [12; 13; 14; 15; 16; 17]. The teacher model serves as a temporally smoothed, lagging version of the student model. By training the student with pseudo-labels generated by the teacher, the model is encouraged to maintain temporal consistency on the unlabeled samples.

In this work, it is found that the MT strategy implicitly introduces a mechanism similar to self-paced learning [18]. Taking a supervised learning task using the MT strategy as an example, let \mathbf{y}_{gt} denote the ground truth segmentation label of a sample \mathbf{x} , $\hat{\mathbf{y}}$ the student output, and $\hat{\mathbf{y}}_t$ the teacher-generated pseudo-label. The training objective for the student is

$$\mathcal{L} = \mathcal{L}(\hat{\mathbf{y}}, \mathbf{y}_{\text{gt}}) + \lambda \mathcal{L}(\hat{\mathbf{y}}, \hat{\mathbf{y}}_t), \quad (2)$$

which can be reformulated based on whether the teacher’s prediction agrees with the ground truth, i.e., $\hat{\mathbf{y}}_t = \mathbf{y}_{\text{gt}}$

$$\mathcal{L} = \mathbb{I}(\hat{\mathbf{y}}_t = \mathbf{y}_{\text{gt}})(\mathcal{L}(\hat{\mathbf{y}}, \mathbf{y}_{\text{gt}}) + \lambda \mathcal{L}(\hat{\mathbf{y}}, \hat{\mathbf{y}}_t)) + \mathbb{I}(\hat{\mathbf{y}}_t \neq \mathbf{y}_{\text{gt}})(\mathcal{L}(\hat{\mathbf{y}}, \mathbf{y}_{\text{gt}}) + \lambda \mathcal{L}(\hat{\mathbf{y}}, \hat{\mathbf{y}}_t)), \quad (3)$$

$$= \mathbb{I}(\hat{\mathbf{y}}_t = \mathbf{y}_{\text{gt}})(1 + \lambda)\mathcal{L}(\hat{\mathbf{y}}, \mathbf{y}_{\text{gt}}) + \mathbb{I}(\hat{\mathbf{y}}_t \neq \mathbf{y}_{\text{gt}})(\mathcal{L}(\hat{\mathbf{y}}, \mathbf{y}_{\text{gt}}) + \lambda \mathcal{L}(\hat{\mathbf{y}}, \hat{\mathbf{y}}_t)), \quad (4)$$

where \mathbb{I} is the indicator function, applied pixel-wise, that activates the corresponding term based on whether $\hat{\mathbf{y}}_t$ matches ground truth \mathbf{y}_{gt} . When the temporally lagged teacher label agrees with the ground truth, the loss simplifies to

$$\mathcal{L} = (1 + \lambda)\mathcal{L}(\hat{\mathbf{y}}, \mathbf{y}_{\text{gt}}), \quad (5)$$

indicating reinforcement of the ground truth signal. When the teacher-generated label disagrees with the ground truth, the loss becomes

$$\mathcal{L} = \mathcal{L}(\hat{\mathbf{y}}, \mathbf{y}_{\text{gt}}) + \lambda \mathcal{L}(\hat{\mathbf{y}}, \hat{\mathbf{y}}_t), \quad (6)$$

which reflects competing gradients from two sources, balancing the optimization of $\hat{\mathbf{y}}$ in different directions.

Based on this analysis, we speculate that the pseudo-labels generated by the temporally lagged teacher model control the pace of the learning process. During the early epochs of training, the teacher model tends to make confident predictions on easier regions, causing the optimization target Equation (2) to focus more on these simpler tasks. As training progresses, the agreement between the teacher model and the ground truth gradually extends to more difficult regions, thereby guiding the student model to tackle increasingly challenging examples.

To verify this assumption, we conduct supervised learning experiments using the MT strategy with 100% labeled data from the ACDC and Promise12 datasets. As shown in Table 1, simply applying the MT strategy to supervised segmentation improves model performance. Note that this setting does not involve learning from unlabeled data. Figure 1 presents the agreement between teacher-generated labels and ground truth labels across training iterations in supervised segmentation with the MT strategy. The results illustrate that the regions of agreement expand from the object center to the borders as training progresses, partially confirming the hypothesis that the MT strategy controls the pace of the learning process.

Table 1: Preliminary results on supervised segmentation with/without the MT strategy. The MT strategy enhances performance in supervised learning.

	ACDC				Promise12	
	DSC \uparrow	Jaccard \uparrow	95HD \downarrow	ASD \downarrow	DSC \uparrow	ASD \downarrow
U-Net (w/o MT)	91.44	84.59	4.30	0.99	84.76	1.58
U-Net (w/ MT)	91.70	85.02	1.15	0.29	85.22	1.55

Instead of using a temporally lagged model to regulate the pace of learning, as in the MT strategy, we introduce generalized models that differs from the student not only in temporally lagged parameters but also in architectures. By tuning the associated hyperparameters, this method gains flexibility in producing signals that are temporally lagged or cross-architectural, providing greater freedom in controlling the pace of learning. Moreover, the proposed strategy is more easily extended to the unsupervised setting, as it no longer requires ground truth labels to regulate the learning process.

Specifically, a novel framework called dual teacher student learning (DTSL) is proposed, which consists of two groups of teacher-student models. In each group, the teacher and student share

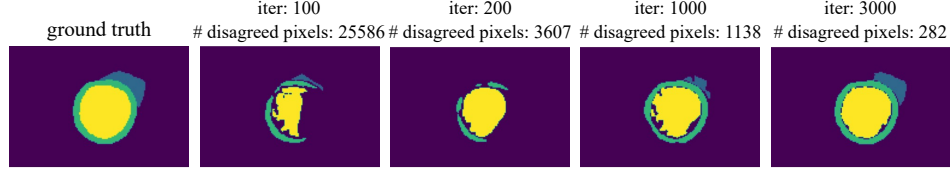


Figure 1: The agreement between teacher-generated labels and ground truth labels across training iterations in supervised segmentation with the MT strategy. The regions of agreement expand from the object center to the borders as training progresses.

the same architecture, and the teacher is updated via an EMA of the student’s weights. For each student, both its corresponding teacher and the student model from the other group regulate the pace of learning by using the agreement of their outputs as pseudo-labels. To precisely control the learning pace, a method called the consensus label generator (CLG) is proposed, which generates pseudo-labels based on the Jensen-Shannon (JS) divergence [19] between model outputs.

The main contributions of this work are as follows:

- This is the first work to interpret the MT strategy from the perspective of self-paced learning.
- A novel framework, consisting of DTSL and CLG, is proposed to extend self-pace learning from being regulated solely by a temporally lagged teacher to being guided by both temporally lagged and cross-architectural models. This provides greater flexibility in controlling the pace of learning and enhances model performance.

Extensive experiments across various mainstream methods and datasets demonstrate that the proposed DTSL framework outperforms state-of-the-art (SOTA) approaches in both supervised and semi-supervised medical image segmentation. Ablation studies and hyperparameter optimization further validate the effectiveness of the proposed method.

2 Related Works

2.1 Medical image segmentation

Contemporary medical image segmentation aims to delineate regions of interest across various imaging modalities, such as magnetic resonance imaging (MRI) and computed tomography (CT) [20; 21; 22; 23]. UNet[1] has served as a foundational architecture in this domain, and much subsequent research has focused on improving its adaptability and performance. Examples include extending UNet to 3D structures [24], introducing residual connections to enhance learning performance [25], and integrating transformer layers with convolutional blocks for better feature extraction [26]. Nevertheless, a major limitation of medical image segmentation lies in its reliance on large quantities of precise, high-quality annotations, an effort that demands substantial time and expertise [4].

2.2 Self-paced learning

Self-paced learning [18] is a learning methodology inspired by cognitive science, which cautiously and adaptively prioritizes learning from simple and reliable examples, and gradually transitions to more difficult ones. Common self-paced learning methods [27; 28] are capable of autonomously evaluating the difficulty of samples, making the learning process dynamic and optimizable. Self-paced learning has been successfully applied to a variety of tasks, achieving strong performance in areas such as saliency detection [29] and object tracking[30].

2.3 Semi-supervised learning

Semi-supervised learning aims to train models using a combination of labeled and unlabeled data [7; 9]. The main approaches include pseudo-labeling, consistency regularization, and entropy minimization. Pseudo-labeling methods [31; 32] first perform supervised learning on labeled data, then generate pseudo-labels for unlabeled data, and finally refine these pseudo-labels using strategies such as random propagation. Consistency regularization methods [33; 34; 35] enforce the model to

produce consistent predictions on unlabeled data under various perturbations. Entropy minimization methods [36; 37] aim to minimize the output entropy of the model for unlabeled samples.

A widely adopted strategy in semi-supervised learning is the MT framework [12], which encourages the student model to produce predictions consistent with those of the teacher model. This approach has inspired numerous successful algorithms. For example, UA-MT[38] leverages uncertainty information to guide the student model to gradually learn from the reliable predictions of the teacher. Tri-U-MT[39] introduces a triple uncertainty-guided MT framework, incorporating two auxiliary tasks, reconstructing and predicting signed distance fields on top of the MT to reduce learning divergence and improve prediction performance.

2.4 Co-learning

Co-learning has also proven to be an effective approach in SSMIS [40; 41]. It typically involves two sub-networks with similar yet distinct architectures that generate pseudo-labels for each other, enabling both models to iteratively learn more representative features from unlabeled data. CrossTeaching[42] allows two distinct self-supervised networks to generate pseudo-labels for unlabeled samples and perform cross-pseudo supervision. Semi-CML[8] proposed a semi-supervised contrastive mutual learning segmentation framework, which effectively leverages cross-modal information and prediction consistency between different modalities for mutual contrastive learning. SDCL[43] introduces a new architecture consisting of one teacher model and two student models, designed to reduce errors during training by improving model collaboration and robustness.

3 Method

3.1 Problem setting

In semi-supervised segmentation, the training set D consists of two parts, a labeled dataset $D^\ell = \{(\mathbf{x}_i^\ell, \mathbf{y}_i^\ell)\}_{i=1}^N$ and an unlabeled dataset $D^u = \{\mathbf{x}_i^u\}_{i=N+1}^{M+N}$, where $N \ll M$. Each labeled medical image $\mathbf{x}_i^\ell \in \mathbb{R}^{H \times M}$ in D^ℓ is associated with a label $\mathbf{y}_i^\ell \in \{0, 1, \dots, K-1\}^{H \times M}$, where K is the number of classes and class 0 denotes the background.

The goal of semi-supervised learning is to perform supervised learning on D^ℓ , while also leveraging the unlabeled dataset D^u , in order to make accurate predictions on a test set $D^t = \{(\mathbf{x}_i^t, \mathbf{y}_i^t)\}$ with ground truth labels.

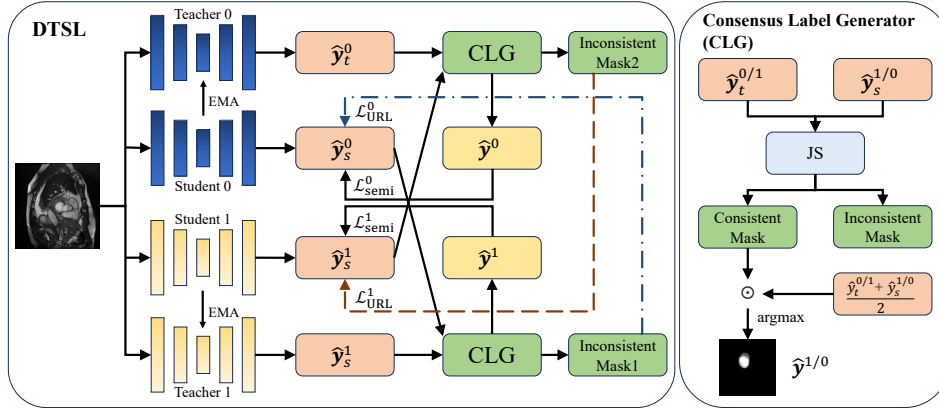


Figure 2: Overview of the DTSL framework for SSMIS. The supervised component is omitted. The associated losses correspond to Equation (18).

3.2 Dual teacher student learning framework

As illustrated in Figure 2, the proposed DTSL framework consists of two groups of teacher-student models, where each group shares the same model architecture. The architectures across the groups are distinct.

During training, the student models are updated via gradient descent-based optimization on a integrated loss function, while the parameters of the teacher models are updated using the EMA strategy defined in Equation (1), based on their respective student models.

The optimization objective for the student models on supervised samples consists of two components

$$\mathcal{L}^\ell = \mathcal{L}_{\text{sup}} + \mathcal{L}_{\text{pace}}, \quad (7)$$

where \mathcal{L}_{sup} is the conventional mixed loss of cross-entropy and Dice loss [44], and $\mathcal{L}_{\text{pace}}$ is the newly introduced loss term that regulates the learning pace. For student_{*i*} from group *i*, (*i* = 0, 1), the supervised loss \mathcal{L}_{sup} is defined as

$$\mathcal{L}_{\text{sup}}^i = \frac{1}{2}(\mathcal{L}_{\text{CE}}(\hat{\mathbf{y}}_s^i, \mathbf{y}_{\text{gt}}) + \mathcal{L}_{\text{dice}}(\hat{\mathbf{y}}_s^i, \mathbf{y}_{\text{gt}})), \quad (8)$$

where $\hat{\mathbf{y}}_s^i$ denotes the prediction of student_{*i*} and \mathbf{y}_{gt} denotes the ground truth label.

For unlabeled samples, only the ‘‘pace regulator’’ $\mathcal{L}_{\text{pace}}$ is used to update the student model

$$\mathcal{L}^u = \mathcal{L}_{\text{pace}}. \quad (9)$$

In this case, the ‘‘pace regulator’’ $\mathcal{L}_{\text{pace}}$ not only controls the learning pace but also functions similarly to conventional pseudo-label propagation.

3.2.1 Consensus label generator and $\mathcal{L}_{\text{pace}}$

As mentioned in Section 1, the learning pace, originally regulated by the agreement between the temporally lagged teacher model and the ground truth labels, is extended to incorporate the agreement between a temporally lagged model and a cross-architectural model. This is implemented by applying pseudo labels jointly generated based on the consensus of the two respective models, referred to as the CLG.

Given two different models, typically the student and teacher models across groups by default, let \mathbf{o}_1 and \mathbf{o}_2 denote their outputs, which are tensors representing categorical distribution predictions for segmentation labels. The consistency between \mathbf{o}_1 and \mathbf{o}_2 is used as the pseudo-label for the other student model, as illustrated in Figure 2.

Specifically, the JS divergence [19] is computed along the distribution axis of \mathbf{o}_1 and \mathbf{o}_2

$$\text{JS}(\mathbf{o}_1, \mathbf{o}_2) = \frac{1}{2}\text{KL}(\mathbf{o}_1 || \mathbf{m}) + \frac{1}{2}\text{KL}(\mathbf{o}_2 || \mathbf{m}), \quad (10)$$

where $\mathbf{m} = \frac{\mathbf{o}_1 + \mathbf{o}_2}{2}$. JS divergence is a symmetric measure of similarity between two distributions, derived from the Kullback–Leibler (KL) divergence [45]. It ranges from 0 to 1 when base-2 logarithm is used. In the next, a threshold $\kappa \in [0, 1]$ is applied to the JS divergence to divide the segmentation map into consistent and inconsistent parts

$$\text{Mask}_{\text{cons}} = \mathbb{1}(\text{JS}(\mathbf{o}_1, \mathbf{o}_2) < \kappa); \quad (11)$$

$$\text{Mask}_{\text{diff}} = \mathbb{1}(\text{JS}(\mathbf{o}_1, \mathbf{o}_2) \geq \kappa), \quad (12)$$

where $\mathbb{1}$ denotes the indicator function that returns 1 if the condition is true and 0, applied pixel-wise. For consistent regions (easy regions), the CLG generates pseudo-labels using the intermediate distributions of the corresponding distributions in \mathbf{o}_1 and \mathbf{o}_2 . For inconsistent regions (difficult regions) the background class is assigned directly

$$\text{CLG}(\mathbf{o}_1, \mathbf{o}_2) = \text{argmax} \left(\frac{\mathbf{o}_1 + \mathbf{o}_2}{2} \odot \text{Mask}_{\text{cons}} + \text{onehot}(\mathbf{0}) \odot \text{Mask}_{\text{diff}} \right) \quad (13)$$

This approach generates pseudo-labels in a self-paced manner, starting from easy regions and gradually incorporating harder regions as training progresses.

Denote the predictions made by student_{*i*} and teacher_{*i*} as $\hat{\mathbf{y}}_s^i$ and $\hat{\mathbf{y}}_t^i$ respectively, where *i* = 0, 1. As part of $\mathcal{L}_{\text{pace}}$, a semi-supervised loss is defined between the student predictions and the pseudo-labels generated by CLG,

$$\mathcal{L}_{\text{semi}}^0 = \mathcal{L}_{\text{dice}}(\hat{\mathbf{y}}_s^0, \text{CLG}(\hat{\mathbf{y}}_s^1, \hat{\mathbf{y}}_t^0)), \quad (14)$$

$$\mathcal{L}_{\text{semi}}^1 = \mathcal{L}_{\text{dice}}(\hat{\mathbf{y}}_s^1, \text{CLG}(\hat{\mathbf{y}}_s^0, \hat{\mathbf{y}}_t^1)), \quad (15)$$

which aligns with the common use of pseudo-labels in semi-supervised learning frameworks.

Motivate by [43], an extra loss term is applied to the inconsistent regions between a student and its across-group teacher to encourage reconsideration of the discrepant predictions. This loss is implemented by comparing the prediction with a discrete uniform distribution, thereby increasing the entropy of the prediction, and is referred to as the uniform regularization loss (URL). Specifically, taking student₀ as an example, given the predictions $\hat{\mathbf{y}}_s^0$ and $\hat{\mathbf{y}}_t^1$ from student₀ and teacher₁, respectively, the inconsistent regions are calculated as

$$\text{Mask}_{\text{diff}}^0 = \mathbb{1}(\text{JS}(\hat{\mathbf{y}}_s^0, \hat{\mathbf{y}}_t^1) \geq \kappa), \quad (16)$$

and the URL with respect to student₀ is computed as

$$\mathcal{L}_{\text{URL}}^0 = \text{KL}(\hat{\mathbf{y}}_s^0, \text{Uniform}) \odot \text{Mask}_{\text{diff}}^0, \quad (17)$$

where Uniform denotes the discrete uniform distribution over the classes.

Finally, the semi-supervised loss $\mathcal{L}_{\text{semi}}$ along with the URL \mathcal{L}_{URL} together form the pace regulator $\mathcal{L}_{\text{pace}}$ as follows,

$$\mathcal{L}_{\text{pace}} = \alpha \mathcal{L}_{\text{semi}} + \beta \mathcal{L}_{\text{URL}} = \alpha(\mathcal{L}_{\text{semi}}^0 + \mathcal{L}_{\text{semi}}^1) + \beta(\mathcal{L}_{\text{URL}}^0 + \mathcal{L}_{\text{URL}}^1), \quad (18)$$

where α and β are the weighting scalars for the corresponding terms.

Overall, by optimizing the losses proposed in Equation (7) and Equation (9), the proposed DTSL is trained in a self-paced manner, regulated by agreements not only between temporally lagged models but also between cross-architectural models. The testing results outperform the SOTA.

4 Experiments

4.1 Datasets, metrics, and backbone architectures

The DTSL is evaluated on both 2D and 3D datasets, including: ACDC [46], Promise12 [47], LA [48], and Pancreas-NIH [49]. Details of the datasets can be found in Appendix A.

Following previous works [7; 11], four popular evaluation metrics, which are Dice Similarity Coefficient (DSC), Jaccard, 95% Hausdorff Distance (95HD), and Average Surface Distance (ASD), are adopted for the ACDC, LA, and Pancreas-NIH datasets. For the Promise12 dataset, following previous approaches, DSC and ASD are used as evaluation metrics.

For experiments on the 2D datasets, including ACDC and Promise12, the U-Net [1] and ResU-Net [25] are employed as the backbone architectures for the two groups of teacher-student models, respectively. For experiments on the 3D datasets, including LA and Pancreas-NIH, V-Net [24] and ResV-Net [40] are used as the backbone architectures for the two groups of models, respectively.

4.2 Comparison experiments

To investigate the impact of the self-paced learning mechanism on model performance, we conduct experiments using the DTSL framework in a purely supervised setting across the four datasets, using varying proportions of labeled data, as shown in the bottom parts of Tables 2 to 5. These results indicate that DTSL consistently outperforms the standard U-Net/V-Net baselines. Interestingly, when comparing the performance of supervised U-Net/V-Net, supervised DTSL, and semi-supervised DTSL under limited labeled data, the majority of the performance gain is observed in the transition from supervised U-Net/V-Net to supervised DTSL, rather than from supervised DTSL to semi-supervised DTSL. This suggests that the performance improvement is primarily driven by the self-paced learning strategy rather than the incorporation of additional unlabeled data.

ACDC dataset: The proposed approach is compared with several SOTA methods, including DTC [33], URPC [50], MC-Net [51], SS-Net [34], SCP-Net [52], PIGCL [53], BCP [7], ABD [54], and SDCL [43]. Table 2 presents the average segmentation performance across four classes on the ACDC dataset, 5% and 10% labeled data. DTSL method outperforms all SOTA baselines across all four evaluation metrics. Notably, with only 10% labeled data, the proposed approach even surpasses fully supervised methods trained on 100% labeled data in terms of DSC and Jaccard metrics, which is an achievement not matched by any of the compared methods.

Figure 3 presents representative segmentation results on the ACDC dataset under the semi-supervised setting with 10% labeled data. As shown in the figure, the proposed method produces segmentations that align more closely with the ground truth compared to other approaches, particularly in fine structures. Notably, in the red region at the bottom of the figure, only our method achieves accurate segmentation.

Table 2: Comparison with other methods on the ACDC dataset.

	Scans used		Metrics			
	Labeled	Unlabeled	DSC \uparrow	Jaccard \uparrow	95HD \downarrow	ASD \downarrow
DTC (AAAI'2021) [33]	3 (5%)	67 (95%)	56.90	45.67	23.36	7.39
URPC (MICCAI'2021) [50]			55.87	44.64	13.60	3.74
MC-Net (MICCAI'2021) [51]			62.85	52.29	7.62	2.33
SS-Net (MICCAI'2022) [34]			65.83	55.38	6.67	2.28
SCP-Net (MICCAI'2023) [52]			87.27	-	-	2.65
BCP (CVPR'2023) [7]			87.59	78.67	1.90	0.67
ABD(CVPR'2024) [54]			88.96	80.70	1.57	0.52
Ours-DTSL			90.09	82.43	1.74	0.54
DTC (AAAI'2021) [33]	7 (10%)	63 (90%)	84.29	73.92	12.81	4.01
URPC (MICCAI'2021) [50]			83.10	72.41	4.84	1.53
MC-Net (MICCAI'2021) [51]			86.44	77.04	5.50	1.84
SS-Net (MICCAI'2022) [34]			86.78	77.67	6.07	1.40
SCP-Net (MICCAI'2023) [52]			89.69	-	-	0.73
PLGCL (CVPR'2023) [53]			89.1	-	4.98	1.80
BCP (CVPR'2023) [7]			88.84	80.62	3.98	1.17
ABD(CVPR'2024) [54]			89.81	81.95	1.46	0.49
SDCL(MICCAI'2024) [43]			90.92	83.83	1.29	0.34
Ours-DTSL			91.47	84.67	1.10	0.26
U-Net (supervised)	3 (5%)	0	47.83	37.01	31.16	12.62
<i>Ours-DTSL</i> (supervised)	3 (5%)	0	81.36	71.08	6.89	1.56
Ours-DTSL (semi-supervised)	3 (5%)	67 (95%)	90.09	82.43	1.74	0.54
U-Net (supervised)	7 (10%)	0	79.41	68.11	9.35	2.70
<i>Ours-DTSL</i> (supervised)	7 (10%)	0	87.81	79.24	4.55	1.23
Ours-DTSL (semi-supervised)	7 (10%)	63 (90%)	91.47	84.67	1.10	0.26
U-Net (supervised)	70 (All)	0	91.44	84.59	4.30	0.99
<i>Ours-DTSL</i> (supervised)	70 (All)	0	92.22	85.87	1.71	0.41

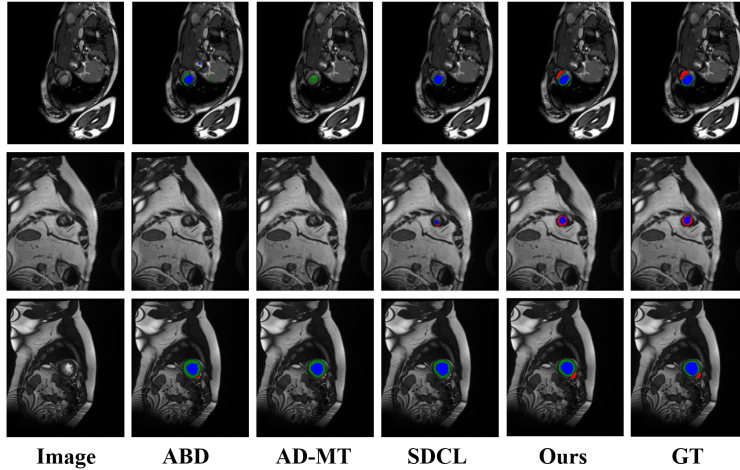


Figure 3: Visualization of segmentation results on ACDC dataset with 10% labeled data

Promise12 dataset: The evaluation results on the Promise12 dataset are summarized in Table 3. Compared with several SOTA methods, including CCT [55], URPC [50], SS-Net [34], SLC-Net [56],

SCP-Net [52], and ABD [54], the proposed approach demonstrates consistent improvements in both DSC and ASD metrics. Notably, in terms of DSC, DTSL achieves a 2.69% improvement over the second-best method, and its ASD is also significantly better than previous methods, demonstrating the superior segmentation accuracy of the proposed approach. Notably, DTSL also outperforms a fully supervised U-Net trained with 100% labeled data, using only 20% labeled samples.

Table 3: Comparison with other methods on the Promise12 dataset.

	Scans used		Metrics	
	Labeled	Unlabeled	DSC↑	ASD↓
CCT (CVPR’2020) [55]			71.43	16.61
URPC (MICCAI’2021) [50]			63.23	4.33
SS-Net (MICCAI’2022) [34]			62.31	4.36
SLC-Net (MICCAI’2022) [56]	7 (20%)	28 (80%)	68.31	4.69
SCP-Net (MICCAI’2023) [52]			77.06	3.52
ABD (CVPR’2024) [54]			82.06	1.33
Ours-DTSL			85.19	0.97
U-Net (supervised)	7 (20%)	0	60.88	13.87
<i>Ours-DTSL</i> (supervised)	7 (20%)	0	81.61	1.16
Ours-DTSL (semi-supervised)	7 (20%)	28 (80%)	85.19	0.97
U-Net (supervised)	35 (All)	0	84.76	1.58
<i>Ours-DTSL</i> (supervised)	35 (All)	0	85.73	0.95

LA dataset: Several SOTA baselines, including UA-MT [38], SASSNet [5], DTC [33], SS-Net [34], PS-MT [17], BCP [7], and AD-MT [54], are compared. As shown in Table 4, the proposed method achieves superior performance in DSC, Jaccard Index, and 95% Hausdorff Distance (95HD), Although the performance on the ASD metric is slightly inferior to AD-MT [54], the overall results demonstrate the effectiveness and robustness of our approach.

Table 4: Comparison with other methods on the LA dataset.

	Scans used		Metrics			
	Labeled	Unlabeled	DSC↑	Jaccard↑	95HD↓	ASD↓
UA-MT (MICCAI’2019) [38]			82.26	70.98	13.71	3.82
SASSNet (MICCAI’2020) [5]			81.60	69.93	16.16	3.58
DTC (AAAI’2021) [33]			81.25	69.33	14.90	3.99
SS-Net (MICCAI’2022) [34]	4 (5%)	76 (95%)	86.33	76.15	9.97	2.31
PS-MT (CVPR’2022) [17]			88.49	79.13	8.12	2.78
BCP (CVPR’2023) [7]			88.02	78.72	7.90	2.15
AD-MT (ECCV’2024) [54]			89.63	81.28	6.56	1.85
Ours-DTSL			90.26	82.31	5.34	1.94
V-Net (supervised)	4 (5%)	0	52.55	39.60	47.05	9.87
<i>Ours-DTSL</i> (supervised)	4 (5%)	0	85.71	76.22	8.60	2.72
Ours-DTSL (semi-supervised)	4 (5%)	76 (95%)	90.26	82.31	5.34	1.94
V-Net (supervised)	80 (All)	0	91.47	84.36	5.48	1.51
<i>Ours-DTSL</i> (supervised)	80 (All)	0	91.64	84.41	5.32	1.41

Pancreas-NIH dataset: Table 5 presents the results on the Pancreas-NIH dataset, comparing the proposed method with several SOTA baselines, including UA-MT [38], SASSNet [5], DTC [33], ASE-Net [57], SS-Net [34], PS-MT [17], BCP [7], and AD-MT [54]. It suggests that DTSL outperforms all these methods across all evaluated metrics. Particularly, the proposed method also surpasses the fully supervised method.

4.3 Ablation studies and hyperparameter optimization

Experiments on the ablation studies of each module proposed in DTSL, different CLG strategy, and optimization of hyperparameters are conducted, on ACDC dataset with 10% labeled data unless otherwise stated. More comprehensive ablation studies can be found in Appendix B.

Table 5: Comparison with other methods on the Pancreas-NIH dataset.

	Scans used		Metrics			
	Labeled	Unlabeled	DSC \uparrow	Jaccard \uparrow	95HD \downarrow	ASD \downarrow
UA-MT (MICCAI'2019) [38]			66.34	53.21	17.21	4.57
SASSNet (MICCAI'2020) [5]			68.78	53.86	19.02	6.26
DTC (AAAI'2021) [33]			69.21	54.06	17.21	5.95
ASE-Net (TMI'2022) [57]			71.54	56.82	16.33	5.73
SS-Net (MICCAI'2022) [34]	6 (10%)	54 (90%)	71.76	57.05	17.56	5.77
PS-MT (CVPR'2022) [17]			76.94	62.73	13.12	3.66
BCP (CVPR'2023) [7]			73.83	59.24	12.71	3.72
AD-MT (ECCV'2024) [54]			80.21	67.51	7.18	1.66
Ours-DTSL			83.07	71.24	4.79	1.30
V-Net (supervised)	6 (10%)	0	55.60	41.74	45.33	18.63
<i>Ours-DTSL</i> (supervised)	6 (10%)	0	73.32	63.42	8.59	5.13
Ours-DTSL (semi-supervised)	6 (10%)	54 (90%)	83.07	71.24	4.79	1.30
V-Net (supervised)	60 (All)	0	82.60	70.81	5.61	1.33
<i>Ours-DTSL</i> (supervised)	60 (All)	0	83.51	71.62	4.71	1.25

Effectiveness of each module in DTSL: Experiments are conducted on a vanilla MT strategy, a dual pseudo-label setup using teacher and across-group student models (Plain DTSL), the use of CLG for pseudo-label generation as described in Equation (13), and the application of URL in Equation (17), with the results presented in Table 6. The results indicate that employing dual groups of teacher-student models significantly outperforms the standard single-group MT approach. Furthermore, incorporating the CLG module substantially enhances performance compared to Plain DTSL. Finally, applying URL on top of CLG provides an additional, though smaller, improvement.

Table 6: Effectiveness of of each module in DTSL.

MT	Plain DTSL	CLG	\mathcal{L}_{URL}	DSC \uparrow	Jaccard \uparrow	95HD \downarrow	ASD \downarrow
\checkmark				80.10	75.60	4.31	2.33
	\checkmark			89.73	81.97	1.71	0.49
		\checkmark		91.26	84.34	1.40	0.43
	\checkmark		\checkmark	88.65	80.44	2.26	0.67
		\checkmark	\checkmark	91.47	84.67	1.10	0.26

Table 7: Results of different strategies of CLG.

Strategy	DSC \uparrow	Jaccard \uparrow	95HD \downarrow	ASD \downarrow
Strategy 1	90.21	82.69	1.70	0.53
Strategy 2	90.45	83.21	1.98	0.41
Strategy 3	90.64	83.29	1.60	0.30
Default	91.47	84.67	1.10	0.26

Table 8: Optimization of the hyperparameter κ .

κ	DSC \uparrow	Jaccard \uparrow	95HD \downarrow	ASD \downarrow
0.01	87.83	74.97	1.75	0.41
0.05	91.47	84.67	1.10	0.26
0.1	91.12	84.08	2.53	0.57
0.15	91.01	83.97	1.94	0.51

Results of different CLG strategies: Taking student₀ as an example, the proposed method (default) generates pseudo-labels using outputs from teacher₀ and student₁ via the CLG module. We also explore alternative strategies: using teacher₁ and student₁ to generate pseudo-labels for student₀ (Strategy 1), using teacher₀ and teacher₁ to generate pseudo-labels for student₀ (Strategy 2), and using triple outputs of teacher₀, teacher₁, and student₁ to generate pseudo-labels for student₀ (Strategy 3). The training process for student₁ follows a similar setup. As shown in Table 7, the default setting achieves the best performance among all strategies.

Optimization of the threshold κ : The threshold κ , introduced in Equation (11), is used to filter out inconsistent regions based on the JS divergence. Since the consistent regions are critical for regulating the pace of learning in this method, the hyperparameter κ plays a vital role. Experimental results, presented in Table 8, show that performance first increases and then decreases with varying κ , reaching a peak at $\kappa = 0.05$.

More in Appendix B: The optimization of ω in Equation (1), experiments on alternative architecture combinations, the optimization of κ under additional settings, and the tuning of α, β in Equation (18) are presented in Appendix B.

References

- [1] O. Ronneberger, P. Fischer, and T. Brox, “U-net: Convolutional networks for biomedical image segmentation,” in *Medical image computing and computer-assisted intervention—MICCAI 2015: 18th international conference, Munich, Germany, October 5–9, 2015, proceedings, part III 18*, pp. 234–241, Springer, 2015.
- [2] H. Cao, Y. Wang, J. Chen, D. Jiang, X. Zhang, Q. Tian, and M. Wang, “Swin-unet: Unet-like pure transformer for medical image segmentation,” in *European conference on computer vision*, pp. 205–218, Springer, 2022.
- [3] J. M. J. Valanarasu and V. M. Patel, “Unext: Mlp-based rapid medical image segmentation network,” in *International conference on medical image computing and computer-assisted intervention*, pp. 23–33, Springer, 2022.
- [4] N. Tajbakhsh, L. Jeyaseelan, Q. Li, J. N. Chiang, Z. Wu, and X. Ding, “Embracing imperfect datasets: A review of deep learning solutions for medical image segmentation,” *Medical image analysis*, vol. 63, p. 101693, 2020.
- [5] S. Li, C. Zhang, and X. He, “Shape-aware semi-supervised 3d semantic segmentation for medical images,” in *Medical Image Computing and Computer Assisted Intervention—MICCAI 2020: 23rd International Conference, Lima, Peru, October 4–8, 2020, Proceedings, Part I 23*, pp. 552–561, Springer, 2020.
- [6] H. Wu, Z. Wang, Y. Song, L. Yang, and J. Qin, “Cross-patch dense contrastive learning for semi-supervised segmentation of cellular nuclei in histopathologic images,” in *Proceedings of the IEEE/CVF Conference on Computer Vision and Pattern Recognition*, pp. 11666–11675, 2022.
- [7] Y. Bai, D. Chen, Q. Li, W. Shen, and Y. Wang, “Bidirectional copy-paste for semi-supervised medical image segmentation,” in *Proceedings of the IEEE/CVF conference on computer vision and pattern recognition*, pp. 11514–11524, 2023.
- [8] S. Zhang, J. Zhang, B. Tian, T. Lukasiewicz, and Z. Xu, “Multi-modal contrastive mutual learning and pseudo-label re-learning for semi-supervised medical image segmentation,” *Medical Image Analysis*, vol. 83, p. 102656, 2023.
- [9] J. He, C. Cai, Q. Li, and A. J. Ma, “Pair shuffle consistency for semi-supervised medical image segmentation,” in *International Conference on Medical Image Computing and Computer-Assisted Intervention*, pp. 489–499, Springer, 2024.
- [10] Y. Shi, J. Zhang, T. Ling, J. Lu, Y. Zheng, Q. Yu, L. Qi, and Y. Gao, “Inconsistency-aware uncertainty estimation for semi-supervised medical image segmentation,” *IEEE transactions on medical imaging*, vol. 41, no. 3, pp. 608–620, 2021.
- [11] H. Chi, J. Pang, B. Zhang, and W. Liu, “Adaptive bidirectional displacement for semi-supervised medical image segmentation,” in *Proceedings of the IEEE/CVF conference on computer vision and pattern recognition*, pp. 4070–4080, 2024.
- [12] A. Tarvainen and H. Valpola, “Mean teachers are better role models: Weight-averaged consistency targets improve semi-supervised deep learning results,” *Advances in neural information processing systems*, vol. 30, 2017.
- [13] H. Su, X. Shi, J. Cai, and L. Yang, “Local and global consistency regularized mean teacher for semi-supervised nuclei classification,” in *International Conference on Medical Image Computing and Computer-Assisted Intervention*, pp. 559–567, Springer, 2019.
- [14] S. Li, Z. Zhao, K. Xu, Z. Zeng, and C. Guan, “Hierarchical consistency regularized mean teacher for semi-supervised 3d left atrium segmentation,” in *2021 43rd Annual International Conference of the IEEE Engineering in Medicine & Biology Society (EMBC)*, pp. 3395–3398, IEEE, 2021.
- [15] C. Tan, Z. Gao, L. Wu, S. Li, and S. Z. Li, “Hyperspherical consistency regularization,” in *Proceedings of the IEEE/CVF conference on computer vision and pattern recognition*, pp. 7244–7255, 2022.
- [16] Y. Fan, A. Kukleva, D. Dai, and B. Schiele, “Revisiting consistency regularization for semi-supervised learning,” *International Journal of Computer Vision*, vol. 131, no. 3, pp. 626–643, 2023.

- [17] Y. Liu, Y. Tian, Y. Chen, F. Liu, V. Belagiannis, and G. Carneiro, "Perturbed and strict mean teachers for semi-supervised semantic segmentation," in *Proceedings of the IEEE/CVF conference on computer vision and pattern recognition*, pp. 4258–4267, 2022.
- [18] M. Kumar, B. Packer, and D. Koller, "Self-paced learning for latent variable models," *Advances in neural information processing systems*, vol. 23, 2010.
- [19] J. Lin, "Divergence measures based on the shannon entropy," *IEEE Transactions on Information Theory*, vol. 37, no. 1, pp. 145–151, 1991.
- [20] Ö. Çiçek, A. Abdulkadir, S. S. Lienkamp, T. Brox, and O. Ronneberger, "3d u-net: learning dense volumetric segmentation from sparse annotation," in *Medical Image Computing and Computer-Assisted Intervention–MICCAI 2016: 19th International Conference, Athens, Greece, October 17–21, 2016, Proceedings, Part II 19*, pp. 424–432, Springer, 2016.
- [21] Q. Dou, Q. Liu, P. A. Heng, and B. Glocker, "Unpaired multi-modal segmentation via knowledge distillation," *IEEE transactions on medical imaging*, vol. 39, no. 7, pp. 2415–2425, 2020.
- [22] X. Li, H. Chen, X. Qi, Q. Dou, C.-W. Fu, and P.-A. Heng, "H-denseunet: hybrid densely connected unet for liver and tumor segmentation from ct volumes," *IEEE transactions on medical imaging*, vol. 37, no. 12, pp. 2663–2674, 2018.
- [23] F. Wang, K. Zheng, L. Lu, J. Xiao, M. Wu, and S. Miao, "Automatic vertebra localization and identification in ct by spine rectification and anatomically-constrained optimization," in *Proceedings of the IEEE/CVF conference on computer vision and pattern recognition*, pp. 5280–5288, 2021.
- [24] A. Abdollahi, B. Pradhan, and A. Alamri, "Vnet: An end-to-end fully convolutional neural network for road extraction from high-resolution remote sensing data," *Ieee Access*, vol. 8, pp. 179424–179436, 2020.
- [25] F. I. Diakogiannis, F. Waldner, P. Caccetta, and C. Wu, "Resunet-a: A deep learning framework for semantic segmentation of remotely sensed data," *ISPRS Journal of Photogrammetry and Remote Sensing*, vol. 162, pp. 94–114, 2020.
- [26] J. Chen, Y. Lu, Q. Yu, X. Luo, E. Adeli, Y. Wang, L. Lu, A. L. Yuille, and Y. Zhou, "Transunet: Transformers make strong encoders for medical image segmentation," *arXiv preprint arXiv:2102.04306*, 2021.
- [27] L. Jiang, D. Meng, S.-I. Yu, Z. Lan, S. Shan, and A. G. Hauptmann, "Self-paced learning with diversity," *Advances in neural information processing systems*, vol. 27, 2014.
- [28] L. Jiang, D. Meng, Q. Zhao, S. Shan, and A. Hauptmann, "Self-paced curriculum learning," in *Proceedings of the AAAI Conference on Artificial Intelligence*, vol. 29, 2015.
- [29] D. Zhang, D. Meng, and J. Han, "Co-saliency detection via a self-paced multiple-instance learning framework," *IEEE transactions on pattern analysis and machine intelligence*, vol. 39, no. 5, pp. 865–878, 2016.
- [30] J. S. Supancic and D. Ramanan, "Self-paced learning for long-term tracking," in *Proceedings of the IEEE conference on computer vision and pattern recognition*, pp. 2379–2386, 2013.
- [31] H. Yao, X. Hu, and X. Li, "Enhancing pseudo label quality for semi-supervised domain-generalized medical image segmentation," in *Proceedings of the AAAI conference on artificial intelligence*, vol. 36, pp. 3099–3107, 2022.
- [32] J. Wang and T. Lukasiewicz, "Rethinking bayesian deep learning methods for semi-supervised volumetric medical image segmentation," in *Proceedings of the IEEE/CVF Conference on Computer Vision and Pattern Recognition*, pp. 182–190, 2022.
- [33] X. Luo, J. Chen, T. Song, and G. Wang, "Semi-supervised medical image segmentation through dual-task consistency," in *Proceedings of the AAAI conference on artificial intelligence*, vol. 35, pp. 8801–8809, 2021.
- [34] Y. Wu, Z. Wu, Q. Wu, Z. Ge, and J. Cai, "Exploring smoothness and class-separation for semi-supervised medical image segmentation," in *International conference on medical image computing and computer-assisted intervention*, pp. 34–43, Springer, 2022.
- [35] C. Xu, Y. Yang, Z. Xia, B. Wang, D. Zhang, Y. Zhang, and S. Zhao, "Dual uncertainty-guided mixing consistency for semi-supervised 3d medical image segmentation," *IEEE Transactions on Big Data*, vol. 9, no. 4, pp. 1156–1170, 2023.

- [36] W. Hang, W. Feng, S. Liang, L. Yu, Q. Wang, K.-S. Choi, and J. Qin, "Local and global structure-aware entropy regularized mean teacher model for 3d left atrium segmentation," in *Medical Image Computing and Computer Assisted Intervention–MICCAI 2020: 23rd International Conference, Lima, Peru, October 4–8, 2020, Proceedings, Part I* 23, pp. 562–571, Springer, 2020.
- [37] S. Vesal, M. Gu, R. Kosti, A. Maier, and N. Ravikumar, "Adapt everywhere: unsupervised adaptation of point-clouds and entropy minimization for multi-modal cardiac image segmentation," *IEEE Transactions on Medical Imaging*, vol. 40, no. 7, pp. 1838–1851, 2021.
- [38] L. Yu, S. Wang, X. Li, C.-W. Fu, and P.-A. Heng, "Uncertainty-aware self-ensembling model for semi-supervised 3d left atrium segmentation," in *Medical image computing and computer assisted intervention–MICCAI 2019: 22nd international conference, Shenzhen, China, October 13–17, 2019, proceedings, part II* 22, pp. 605–613, Springer, 2019.
- [39] K. Wang, B. Zhan, C. Zu, X. Wu, J. Zhou, L. Zhou, and Y. Wang, "Tripled-uncertainty guided mean teacher model for semi-supervised medical image segmentation," in *Medical Image Computing and Computer Assisted Intervention–MICCAI 2021: 24th International Conference, Strasbourg, France, September 27–October 1, 2021, Proceedings, Part II* 24, pp. 450–460, Springer, 2021.
- [40] Y. Wang, B. Xiao, X. Bi, W. Li, and X. Gao, "Mcf: Mutual correction framework for semi-supervised medical image segmentation," in *Proceedings of the IEEE/CVF conference on computer vision and pattern recognition*, pp. 15651–15660, 2023.
- [41] S. Gao, Z. Zhang, J. Ma, Z. Li, and S. Zhang, "Correlation-aware mutual learning for semi-supervised medical image segmentation," in *International Conference on Medical Image Computing and Computer-Assisted Intervention*, pp. 98–108, Springer, 2023.
- [42] X. Luo, M. Hu, T. Song, G. Wang, and S. Zhang, "Semi-supervised medical image segmentation via cross teaching between cnn and transformer," in *International conference on medical imaging with deep learning*, pp. 820–833, PMLR, 2022.
- [43] B. Song and Q. Wang, "Sdcl: Students discrepancy-informed correction learning for semi-supervised medical image segmentation," in *International Conference on Medical Image Computing and Computer-Assisted Intervention*, pp. 567–577, Springer, 2024.
- [44] C. H. Sudre, W. Li, T. Vercauteren, S. Ourselin, and M. Jorge Cardoso, "Generalised dice overlap as a deep learning loss function for highly unbalanced segmentations," in *Deep Learning in Medical Image Analysis and Multimodal Learning for Clinical Decision Support: Third International Workshop, DLMIA 2017, and 7th International Workshop, ML-CDS 2017, Held in Conjunction with MICCAI 2017, Québec City, QC, Canada, September 14, Proceedings 3*, pp. 240–248, Springer, 2017.
- [45] S. Kullback and R. A. Leibler, "On information and sufficiency," *The annals of mathematical statistics*, vol. 22, no. 1, pp. 79–86, 1951.
- [46] O. Bernard, A. Lalande, C. Zotti, F. Cervenansky, X. Yang, P.-A. Heng, I. Cetin, K. Lekadir, O. Camara, M. A. G. Ballester, *et al.*, "Deep learning techniques for automatic mri cardiac multi-structures segmentation and diagnosis: is the problem solved?," *IEEE transactions on medical imaging*, vol. 37, no. 11, pp. 2514–2525, 2018.
- [47] G. Litjens, R. Toth, W. Van De Ven, C. Hoeks, S. Kerkstra, B. Van Ginneken, G. Vincent, G. Guillard, N. Birbeck, J. Zhang, *et al.*, "Evaluation of prostate segmentation algorithms for mri: the promise12 challenge," *Medical image analysis*, vol. 18, no. 2, pp. 359–373, 2014.
- [48] Z. Xiong, Q. Xia, Z. Hu, N. Huang, C. Bian, Y. Zheng, S. Vesal, N. Ravikumar, A. Maier, X. Yang, P.-A. Heng, D. Ni, C. Li, Q. Tong, W. Si, E. Puybareau, Y. Khoudli, T. Géraud, C. Chen, W. Bai, D. Rueckert, L. Xu, X. Zhuang, X. Luo, S. Jia, M. Sermesant, Y. Liu, K. Wang, D. Borra, A. Masci, C. Corsi, C. de Vente, M. Veta, R. Karim, C. J. Preetha, S. Engelhardt, M. Qiao, Y. Wang, Q. Tao, M. Nuñez-Garcia, O. Camara, N. Savioli, P. Lamata, and J. Zhao, "A global benchmark of algorithms for segmenting the left atrium from late gadolinium-enhanced cardiac magnetic resonance imaging," *Medical Image Analysis*, vol. 67, p. 101832, 2021.
- [49] H. R. Roth, L. Lu, A. Farag, H.-C. Shin, J. Liu, E. B. Turkbey, and R. M. Summers, "Deeporgan: Multi-level deep convolutional networks for automated pancreas segmentation," in *Medical Image Computing and Computer-Assisted Intervention – MICCAI 2015* (N. Navab, J. Hornegger, W. M. Wells, and A. Frangi, eds.), (Cham), pp. 556–564, Springer International Publishing, 2015.

- [50] X. Luo, W. Liao, J. Chen, T. Song, Y. Chen, S. Zhang, N. Chen, G. Wang, and S. Zhang, "Efficient semi-supervised gross target volume of nasopharyngeal carcinoma segmentation via uncertainty rectified pyramid consistency," in *Medical Image Computing and Computer Assisted Intervention–MICCAI 2021: 24th International Conference, Strasbourg, France, September 27–October 1, 2021, Proceedings, Part II* 24, pp. 318–329, Springer, 2021.
- [51] Y. Wu, M. Xu, Z. Ge, J. Cai, and L. Zhang, "Semi-supervised left atrium segmentation with mutual consistency training," in *Medical image computing and computer assisted intervention–MICCAI 2021: 24th international conference, Strasbourg, France, September 27–October 1, 2021, proceedings, part II* 24, pp. 297–306, Springer, 2021.
- [52] Z. Zhang, R. Ran, C. Tian, H. Zhou, X. Li, F. Yang, and Z. Jiao, "Self-aware and cross-sample prototypical learning for semi-supervised medical image segmentation," in *International Conference on Medical Image Computing and Computer-Assisted Intervention*, pp. 192–201, Springer, 2023.
- [53] H. Basak and Z. Yin, "Pseudo-label guided contrastive learning for semi-supervised medical image segmentation," in *Proceedings of the IEEE/CVF conference on computer vision and pattern recognition*, pp. 19786–19797, 2023.
- [54] Z. Zhao, Z. Wang, L. Wang, D. Yu, Y. Yuan, and L. Zhou, "Alternate diverse teaching for semi-supervised medical image segmentation," in *European Conference on Computer Vision*, pp. 227–243, Springer, 2024.
- [55] Y. Ouali, C. Hudelot, and M. Tami, "Semi-supervised semantic segmentation with cross-consistency training," in *Proceedings of the IEEE/CVF conference on computer vision and pattern recognition*, pp. 12674–12684, 2020.
- [56] J. Liu, C. Desrosiers, and Y. Zhou, "Semi-supervised medical image segmentation using cross-model pseudo-supervision with shape awareness and local context constraints," in *International Conference on Medical Image Computing and Computer-Assisted Intervention*, pp. 140–150, Springer, 2022.
- [57] T. Lei, D. Zhang, X. Du, X. Wang, Y. Wan, and A. K. Nandi, "Semi-supervised medical image segmentation using adversarial consistency learning and dynamic convolution network," *IEEE transactions on medical imaging*, vol. 42, no. 5, pp. 1265–1277, 2022.

A Details of the Datasets and implementation of DTSL

A.1 Dataset

The ACDC [46] dataset consists of multi-slice 2D cine cardiac MR images from 100 patients and includes four classes: background, right ventricle, left ventricle, and myocardium. It is split into 70, 20, and 10 patients for training, validation, and testing, respectively. Promise12 [47] is the dataset used in the prostate segmentation challenge at MICCAI 2012, containing 50 MRI scans from 50 patients. We divide them into 35 for training, 5 for validation, and 10 for testing. The LA [48] dataset comprises 100 3D gadolinium-enhanced magnetic resonance image (GE-MRIs) scans with segmentation labels. Among them, 80 are used for training and 20 for test. The Pancreas-NIH [49] dataset is a 3D contrast-enhanced abdominal CT dataset containing 80 volumes with manual annotations. We use 60 volumes for training and 20 for testing.

A.2 Implementation of DTSL

We conducted all experiments using PyTorch and an NVIDIA RTX 3090 GPU. For the 2D datasets, we adopted U-Net and ResU-Net as the backbone architectures, while for the 3D datasets, the V-Net and ResV-Net were engaged. The training was performed for 30k iterations on the 2D datasets and 7.5k iterations on the 3D datasets. The Adam optimizer was used with an initial learning rate $\eta_0 = 1 \times 10^{-3}$, decayed by a poly learning rate scheduler defined as $\eta = \eta_0 \times (1 - \text{iter}/\text{max_iter})^{0.9}$. During training, the 2D inputs were cropped to 256×256 , while the 3D inputs were cropped to $96 \times 96 \times 96$ for Pancreas-NIH and $112 \times 112 \times 80$ for LA.

B More Ablation Studies and Hyperparameter Optimization

Optimization of ω during the EMA process: In the MT framework, the weights of the teacher model are updated via the EMA of the student model’s weights, making the teacher a temporally smoothed and lagged version of the student. From the perspective of self-paced learning regulated by a temporally lagged model, the update factor ω in Equation (1) may play a critical role in controlling the learning pace.

To investigate this effect, we conducted experiments with different ω values ranging from 0.90 to 0.99. The results, presented in Table 9, show that the model achieves optimal performance when ω is set to 0.95. However, the performance variation across different ω values is minimal within the DTSL framework. These experiments were conducted on the ACDC dataset using 10% labeled samples.

Table 9: Results with different ω values ranging from 0.90 to 0.99.

ω	0.90	0.91	0.92	0.93	0.94	0.95	0.96	0.97	0.98	0.99
DSC	91.20	91.12	91.19	91.17	91.15	91.33	91.30	91.29	91.24	91.26

Results on alternative network architectures: To explore the impact of using different network architectures for the two groups of models in DTSL, we conducted experiments with various architecture combinations: U-Net/ResU-Net (default), U-Net/Swin-Unet [2], and ResU-Net/Swin-Unet. The results of these comparisons, presented in Table 10, are based on experiments using 10% labeled samples from the ACDC dataset. As shown in Table 10, the default U-Net/ResU-Net configuration outperforms the alternative combinations.

Table 10: The results of various architecture combinations on 10% labeled samples from the ACDC dataset.

Architectures	DSC \uparrow	Jaccard \uparrow	95HD \downarrow	ASD \downarrow
U-Net/SwinU-net	88.67	80.73	2.81	0.92
ResU-Net/SwinU-net	89.09	81.13	2.67	0.77
U-Net/ResU-net	91.47	84.67	1.10	0.26

Optimization of κ for different datasets: κ represents the threshold used to determine consistency regions based on JS divergence. In the main text, we optimized the threshold selection on the ACDC

dataset. Here, we further present results on additional datasets, including the ACDC dataset with 5% labeled samples, LA dataset with 20% labeled samples, Promise12 dataset with 5% labeled samples, and Pancreas-NIH dataset with 10% labeled samples. The corresponding results are presented in Tables 11 to 14.

As shown in Tables 11 to 14, the optimal value of the hyperparameter κ consistently lies around 0.1 across all four datasets when using the commonly used proportion of labeled samples.

Table 11: Results on different choices of κ on 5% labeled ACDC dataset.

κ	DSC \uparrow	Jaccard \uparrow	95HD \downarrow	ASD \downarrow
0.01	85.03	75.38	3.03	0.76
0.05	89.85	82.11	1.35	0.36
0.1	90.09	82.43	1.74	0.54
0.15	89.32	81.35	2.13	0.62
0.2	89.58	81.76	2.12	0.58

Table 12: Results on different choices of κ on 20% labeled LA dataset.

κ	DSC \uparrow	Jaccard \uparrow	95HD \downarrow	ASD \downarrow
0.05	89.55	81.16	8.91	3.03
0.1	90.26	82.31	5.34	1.94
0.15	89.77	81.50	5.61	2.21
0.2	89.56	81.20	6.42	2.38
0.3	89.57	81.23	6.69	2.26

Table 13: Results on different choices of κ on 5% labeled Promise12 dataset.

κ	DSC \uparrow	Jaccard \uparrow	95HD \downarrow	ASD \downarrow
0.01	81.84	69.55	3.86	1.35
0.05	82.57	70.44	3.41	1.34
0.1	84.28	72.98	2.54	0.94
0.15	85.19	74.35	2.60	0.97
0.2	83.81	72.33	3.75	1.40

Table 14: Results on different choices of κ on 10% labeled Pancreas-NIH dataset.

κ	DSC \uparrow	Jaccard \uparrow	95HD \downarrow	ASD \downarrow
0.05	82.33	70.20	5.19	1.34
0.1	83.07	71.24	4.69	1.30
0.15	82.19	69.98	5.33	1.52
0.2	83.05	71.21	4.94	1.32
0.3	82.78	70.81	4.77	1.26

B.1 Hyperparameter optimization on α and β in Equation (18)

As mentioned in the main text, the loss for the pace regulator $\mathcal{L}_{\text{pace}}$ is defined as

$$\mathcal{L}_{\text{pace}} = \alpha \mathcal{L}_{\text{semi}} + \beta \mathcal{L}_{\text{URL}}, \quad (19)$$

where α, β control the weights of $\mathcal{L}_{\text{semi}}$ and \mathcal{L}_{URL} , respectively. Note that there are no additional weighting parameters in Equations (7) and (9), therefore, both α and β should be tuned as hyperparameters independently.

We conducted experiments on these hyperparameters by fixing one and varying the other. The experimental results are shown in Tables 15 and 16, Tables 17 and 18, Tables 19 and 20, and Tables 21 and 22. The results demonstrate that for commonly used proportions of labeled samples in SSMIS tasks across the four datasets, stable choices for α are around 0.10 or 1.00, while $\beta = 0.05$ appears to be a consistently effective setting for all four datasets.

Table 15: Optimization of α on 10% labeled ACDC dataset.

α	DSC \uparrow	Jaccard \uparrow	95HD \downarrow	ASD \downarrow
0.50	91.18	84.22	1.94	0.45
0.75	91.31	84.40	1.13	0.40
1.0	91.47	84.67	1.10	0.26
1.25	90.71	83.56	1.13	0.32
1.50	90.11	82.66	1.22	0.29

Table 16: Optimization of β on 10% labeled ACDC dataset.

β	DSC \uparrow	Jaccard \uparrow	95HD \downarrow	ASD \downarrow
0.01	90.15	82.95	1.18	0.34
0.05	91.47	84.67	1.10	0.26
0.10	91.32	84.42	1.70	0.38
0.50	90.32	82.28	2.19	0.51
1.00	88.24	79.62	3.66	1.54

Table 17: Optimization of α on 5% labeled LA dataset.

α	DSC \uparrow	Jaccard \uparrow	95HD \downarrow	ASD \downarrow
0.05	90.05	81.99	7.15	2.51
0.10	90.26	82.31	5.34	1.94
0.15	89.61	81.29	6.42	2.05
0.20	89.80	81.60	6.14	2.20
0.30	90.02	81.93	6.20	2.20

Table 18: Optimization of β on 5% labeled LA dataset.

β	DSC \uparrow	Jaccard \uparrow	95HD \downarrow	ASD \downarrow
0.01	90.04	82.01	6.24	2.00
0.05	90.26	82.31	5.34	1.94
0.10	89.54	81.55	6.09	2.17
0.20	89.18	80.37	6.49	2.49
0.30	89.84	81.64	5.94	2.03

Table 19: Optimization of α on 20% labeled Promise12 dataset.

α	DSC \uparrow	Jaccard \uparrow	95HD \downarrow	ASD \downarrow
0.50	84.08	72.73	4.08	1.38
0.75	84.76	73.70	3.09	1.17
1.00	84.69	73.63	2.64	1.05
1.25	85.19	74.35	2.60	0.97
1.50	84.42	73.21	2.66	1.00

Table 20: Optimization of β on 20% labeled Promise12 dataset.

β	DSC \uparrow	Jaccard \uparrow	95HD \downarrow	ASD \downarrow
0.01	83.30	71.53	2.78	1.17
0.05	85.19	74.35	2.60	0.97
0.10	83.84	72.42	3.80	1.30
0.50	77.20	63.23	7.54	2.22
1.00	76.41	62.43	3.96	1.24

Table 21: Optimization of α on 10% labeled Pancreas-NIH dataset.

α	DSC \uparrow	Jaccard \uparrow	95HD \downarrow	ASD \downarrow
0.05	82.52	70.43	4.90	1.26
0.10	83.07	71.24	4.79	1.30
0.15	83.02	71.17	4.70	1.25
0.20	82.80	70.87	4.87	1.26
0.30	82.95	71.10	4.65	1.24

Table 22: Optimization of β on 10% labeled Pancreas-NIH dataset.

β	DSC \uparrow	Jaccard \uparrow	95HD \downarrow	ASD \downarrow
0.01	82.77	70.90	4.69	1.29
0.05	83.07	71.24	4.79	1.30
0.10	82.28	70.10	4.71	1.32
0.20	81.93	69.67	6.37	1.25
0.30	82.18	69.98	4.99	1.21

C Broader Impacts

The proposed semi-supervised framework for medical image segmentation holds the potential to substantially advance clinical workflows and healthcare accessibility. By reducing reliance on large-scale annotated datasets, our method mitigates the labor-intensive and costly process of manual labeling by medical experts, thereby accelerating the deployment of AI-driven diagnostic tools in data-scarce environments. This can be particularly impactful in under-resourced regions, where access to high-quality annotations and radiological expertise is limited.